Detection of spectral line curvature in imaging spectrometer data

Robert A. Neville[*a], Lixin Sun[b], Karl Staenz[a]

[a]Canada Centre for Remote Sensing, Natural Resources Canada,
588 Booth St., Ottawa, ON, Canada K1A 0Y7
[b]Dendron Resource Surveys Inc., Lady Ellen Place,
Ottawa, ON, Canada K1Z 5L9

ABSTRACT

A procedure has been developed to measure the band-centres and bandwidths for imaging spectrometers using data acquired by the sensor in flight. This is done for each across-track pixel, thus allowing the measurement of the instrument's slit curvature or spectral 'smile'. The procedure uses spectral features present in the at-sensor radiance which are common to all pixels in the scene. These are principally atmospheric absorption lines. The band-centre and bandwidth determinations are made by correlating the sensor measured radiance with a modelled radiance, the latter calculated using MODTRAN 4.2. Measurements have been made for a number of instruments including Airborne Visible and Infra-Red Imaging Spectrometer (AVIRIS), SWIR Full Spectrum Imager (SFSI), and Hyperion. The measurements on AVIRIS data were performed as a test of the procedure; since AVIRIS is a whisk-broom scanner it is expected to be free of spectral smile. SFSI is an airborne pushbroom instrument with considerable spectral smile. Hyperion is a satellite pushbroom sensor with a relatively small degree of smile. Measurements of Hyperion were made using three different data sets to check for temporal variations.

Keywords: hyperspectral, spectral smile, Hyperion, AVIRIS, SFSI, spectral calibration

1. INTRODUCTION

Many spectrographs exhibit spectral line curvature, sometimes referred to as slit curvature, and commonly in the remote sensing community as spectral smile or frown. Generally these terms refer to the spatial non-linearity of the monochromatic image of a straight entrance slit as it appears in the focal plane of a spectrograph. There are a number of sources for this effect: spatial distortions caused by the dispersion element, prism or grating, or by aberrations in the collimator and imaging optics. In the case of a grating spectrograph, the spectral line curvature derives from the grating equation, and can be shown to vary as the product of the wavelength, the angular dispersion, and the square of the off-axis field angle.[1]

In an imaging spectrometer employing a two-dimensional detector array, the spectrum is dispersed in one dimension, for example along the columns, and the spatial field is oriented along the rows. Ideally the output of this type of imaging spectrometer consists of two-dimensional (spectral-spatial) frames of data in which all the entries in a given row represent a single band-centre wavelength and bandwidth. However, because the detector elements are arranged on a rectilinear grid, the presence of spectral smile prevents the registration of the monochromatic image of the entrance slit onto the straight rows of detector elements. Calibration of the wavelength distribution across both dimensions of the focal plane gives the band-centre and bandwidth for each detector element in the array. With this information, one could process the spectrum in each column, i.e. each spatial pixel, independently. However, most image analysis systems assume the data are organized in spectral bands which have the same wavelengths for all spatial elements. One potential solution is to resample the image data, based on the wavelength calibration data, to create the ideal output array.

The degree of spectral accuracy required depends upon the spectral gradients exhibited by the measured spectra; steep gradients require high spectral accuracy. Such gradients are most often caused by atmospheric absorption bands; when an atmospheric correction is performed to retrieve surface reflectance, the spectra will exhibit 'spikes' in the neighbourhoods of the absorption features if inaccurate band-centre and bandwidth values are used.

---

[*] robert.neville@ccrs.nrcan.gc.ca

2. METHOD

The method described here uses the atmospheric absorption features combined with selected Fraunhofer lines in the exo-atmospheric irradiance as spectral calibration references. Other methods have been developed which utilise the atmospheric absorption features to perform a spectral calibration.[2,3] These differ from the technique described here in the ways in which the data are conditioned and in the metrics used to compare the measured and reference spectra. The accuracy of the results is dependant upon the validity of the atmospheric absorption model. MODTRAN 4.2 has been used in this work to perform the radiative transfer calculations.[4] From the point of view of the characterization of the instrument, it is important that the reference data are accurate; from the pragmatic view of eliminating the spikes in the derived reflectances, it is important only that the wavelength calibration of the measured image data matches the atmospheric reference data. This method satisfies the latter criteria, if not the former.

Simply stated, the absorption features in the measured radiance are compared to those in a modelled, at-sensor radiance calculated using MODTRAN 4.2. The difficulty is knowing what to use as the target reflectance in the calculation of the modelled radiance. If one had a test area for which the reflectances were known for the whole area, then these could be used. However, since even if the scene were to contain a radiometric validation test site, it will have insufficient spatial extent for most sensors, especially for satellite borne instruments. In the general case, the reflectance spectra are unknown, and one has to calculate them using the sensor signal data. This is done by performing an atmosphere correction to extract the at-ground reflectances, using the sensor's nominal band-centre wavelength and bandwidth values. Because these are in general incorrect, spikes occur in the neighbourhood of the atmospheric features. These are suppressed by spectral smoothing over the affected regions to give approximate reflectance spectra for the scene. These reflectances are then input to the radiance modelling process to achieve the at-sensor modelled radiance spectra. To ensure that the measured spectra have the best possible signal-to-noise ratios, the scene pixels are averaged along-track over a large number of image lines to give a single spectral-spatial radiance frame.

The procedure is carried out on the CCRS Imaging Spectrometer Data Analysis System (ISDAS) which uses a look-up-table (LUT) approach for doing the atmospheric correction.[5] A 'raw' LUT is created for the time, date, location, elevation, and appropriate atmospheric conditions, using the MODTRAN 4.2 radiative transfer code. In the normal atmospheric correction procedure a sensor-specific LUT is created by convolving the band response profiles with the 'raw' LUT values. This 'convolved' LUT is then sampled at a sensor's band wavelength values. In the smile detection procedure, many convolved LUTs are created. First, the convolution is repeated for a range of bandwidths selected by the operator. Then each of these LUTs is sampled for band-centre wavelengths which are shifted by a range of operator selected values. The shift range is adjusted to encompass the anticipated smile amplitude; the shift increment is adjusted to be commensurate with the pixel-to-pixel variation in wavelength shift. These are determined by iteration. The bandwidth increment and range values are chosen in a similar manner.

The absorption features selected for this procedure depend upon the spectral resolution and signal-to-noise of the particular sensor under study. The deeper and better resolved the feature appears in the measured spectra, the lower are the error estimates of the resulting wavelength measurements. The comparison between the measured and modelled radiance spectra is performed separately for each selected absorption feature. The wavelength estimates for each of these features and for each across-track pixel are extended to all elements in the array by interpolation or extrapolation. For this, either a low order polynomial fit or a piecewise linear interpolation is used.

The comparison process calculates the Pearson correlation coefficients for each of the band-centre-shift and bandwidth values; the band-centre and bandwidth combination that gives the maximum correlation value is selected as the 'correct' value. This is performed for each of the selected features and for each across-track pixel, providing the shift, and hence the band-centre wavelength and bandwidth values for each pixel across the sensor's total field of view. To reduce the potential influence of the background scene reflectance, features are chosen which are spectrally narrow or which consist of a number of narrow sub-features, and which are still resolvable by the instrument under study. In addition, both the measured spectra and the modelled spectra are filtered with a high-pass filter before the correlations are performed, again to reduce the influence of the scene reflectance.

This process is repeated, updating the wavelength values with each iteration, until a stable result is obtained. If the pixel-to-pixel uniformity (responsivity) coefficients are not sufficiently accurate to eliminate striping in those bands involved in the feature analyses, errors in the wavelength estimates will result. To cancel these effects and those caused by the discrete shift increment, a low-order polynomial is fitted to the final band-centre and bandwidth values. Normally, a second order polynomial is adequate, and is in keeping with theory for the grating spectrometer case, where a cosine dependence is predicted.[1] This assumes that the angular range (at the grating) is small.

This procedure gives the band-centre wavelength and bandwidth values for all the across-track pixels in the neighbourhoods of the atmospheric and solar absorption features observed in the sensor spectral data. To obtain calibrated values for all bands in the array one can interpolate between the selected feature wavelengths using a fitted low-order polynomial; extrapolation to bands beyond the range spanned by these features must be done with care.

3. RESULTS

Spectral line curvature measurements were made for three sensors: Airborne Visible and Infra-Red Imaging Spectrometer (AVIRIS)[6], SWIR Full Spectrum Imager (SFSI)[7], and Hyperion[8]. For Hyperion, three scenes from different dates and locations were used: Coleambally, Australia, {S34.80° E146.01°}, 12 January 2002; Ranger Mill, Australia, {S12.67° E132.92°}, 30 March 2002; Saskatchewan, Canada, {N50.56° W103.64°}, 20 May 2002. The Coleambally scene consists of a mix of heavily vegetated fields and fields with bare soil; the Ranger Mill region is tropical savannah in which the vegetation is sparse compared with the vegetated fields at Coleambally; the Saskatchewan site consists of fields of bare soil partially covered by crop residue.

3.1 AVIRIS smile test

AVIRIS is a 'whiskbroom' imaging spectrometer instrument. At a given instant in time, it observes a single pixel on the ground, achieving the across-track dimension of the image by means of a scanning mirror. The spectrograph subsystem of AVIRIS consists of four spectrographs, each of which covers a different spectral region; the four spectra are concatenated to create the full-range spectrum covering 370 nm to 2508 nm. It has 224 bands with a nominal bandwidth of 10 nm and a spectral sampling interval of 10 nm. The stated band response profile is Gaussian. Each of the spectrographs disperses its spectrum across a linear detector array. Because each spatial pixel across the swath is observed by the same combination of spectrographs and the same linear detector arrays, one expects the data to be free of spectral smile. This expectation will be
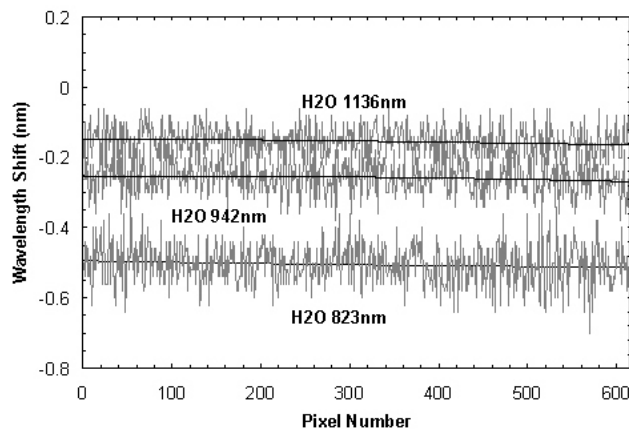

Figure 1a. Measured wavelength shifts for AVIRIS data at the 823 nm, 942 nm, and 1136 nm water vapour bands.
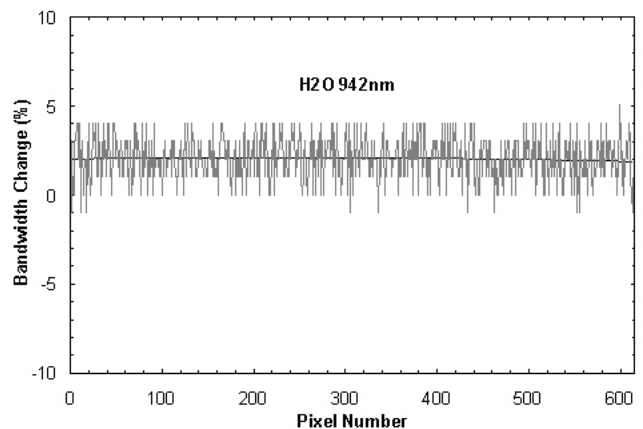
Figure 1b. Measured bandwidth increment for AVIRIS data at the 942 nm water vapour band.

realised only if the scanning operation does not cause any change in the angle or cross-sectional extent and shape of the collimated beam transiting the spectrograph(s).

The AVIRIS data set used for this test was collected over Cuprite, Nevada, in June 1996. This is a desert area containing minimal vegetation, but a wide variety of alteration minerals. Shown in Figure 1a are results obtained for the water vapour absorption lines at 823 nm, 942 nm, and 1136 nm. A second order polynomial has been fitted to the measurements for each pixel across the swath. The standard deviation of the individual measurements relative to the fitted curve are listed in Table 1, as is the standard deviation of the mean fit curve. The mean shift is the difference between the band-centre wavelength, specified in the data set, and the mean of the curve-fit values. The smile amplitude is the maximum curve-fit value minus the minimum. In Figure 1b, the measured values and the corresponding second order polynomial curve fit are plotted for the effective bandwidths of the AVIRIS bands in the neighbourhood of the 942 nm water vapour feature. These are given as the percent change in the nominal specified bandwidths.

Absorption Feature & Wavelength (nm)	H_2O 823	H_2O 942	H_2O 1136
Standard Deviation (nm) (Measurements vs Fit)	0.0598	0.0462	0.0449
Standard Deviation of the Mean Fit (nm)	0.0024	0.0019	0.0018
Mean Shift (nm)	-0.5046	-0.2571	-0.1536
Smile Amplitude (nm)	0.0182	0.0162	0.018

Table 1. Statistics for the spectral smile measurements on the AVIRIS data, for three water vapour features: 823 nm, 942 nm, and 1136 nm.

3.2 SFSI smile measurement

The SFSI sensor is a grating-based, 'pushbroom' imaging spectrometer which acquires the across-track spatial and the spectral dimensions simultaneously; as such it is expected to exhibit spectral line curvature, or spectral smile. SFSI has 234 bands covering the range 1219 nm - 2437 nm with an average spectral sampling interval of 5.2 nm with a nominal bandwidth of 10 nm. In Figure 2 are displayed the results for the oxygen feature at 1268 nm, the small water vapour feature at 1470 nm, and the large carbon dioxide feature at 2007 nm. In total, 9 features across the range from 1268 nm to 2392 nm were measured. The fitted curves have been calculated using second order polynomial fits across-track. In Table 2, the smile amplitude and the mean shift, relative to the specified band-centre value, along with the standard deviation and standard deviation of the mean fit are listed for three of the 9 absorption features.
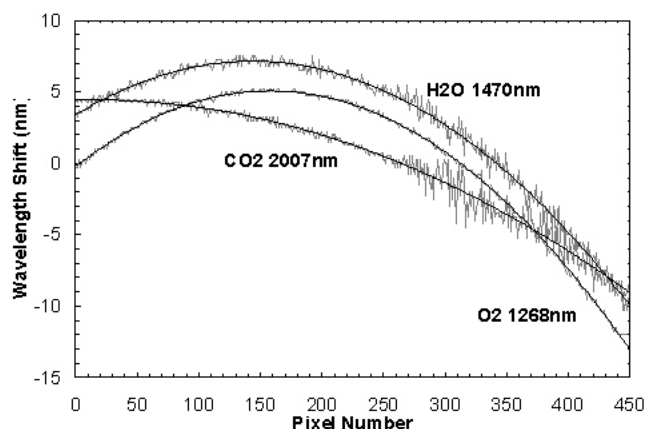

Figure 2. Measured wavelength shifts for SFSI data for atmospheric absorption features at 1268 nm, 1470 nm, and 2007 nm

Absorption Feature & Wavelength (nm)	O_2 1268	H_2O 1470	CO_2 2007
Standard Deviation (nm) (Measurements vs Fit)	0.1659	0.3995	0.5758
Standard Deviation of the Mean Fit (nm)	0.0078	0.0188	0.0271
Mean Shift (nm)	0.5111	2.8533	0.0706
Smile Amplitude (nm)	18.1651	17.1329	13.5136

Table 2. Statistics for the spectral smile measurements made on the SFSI data for three absorption features: oxygen (1268 nm), water vapour (1470 nm), and carbon dioxide (2007 nm)
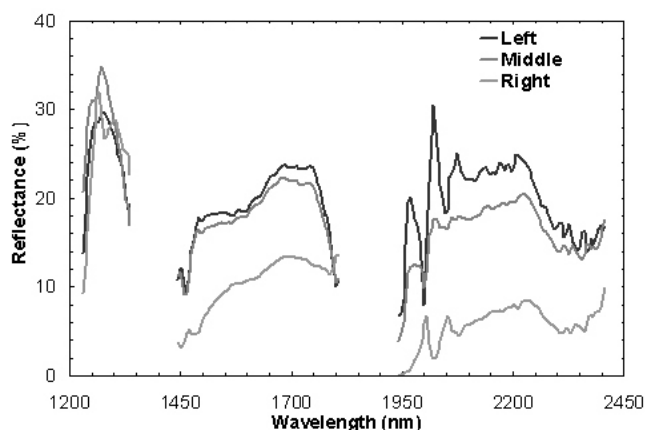
Figure 3a. SFSI reflectance spectra calculated before band-centre and bandwidth corrections.
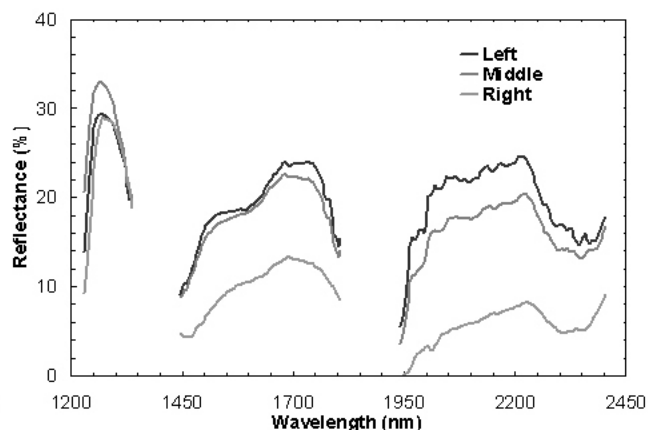
Figure 3b. SFSI reflectance spectra calculated after measured wavelength values were applied.

The across-track second order polynomial curves give the wavelength shifts from which it is a simple matter to calculate the wavelength values for the bands in the neighbourhoods of the measured spectral features. To interpolate, and extrapolate these values to cover all bands within the range of the sensor, a third order polynomial fit of wavelength to band number was performed. Dispersion grating theory suggests that a second order polynomial approximation would suffice for the linear dispersion of a grating instrument. However for this instrument, optical aberrations have contributed to the dispersion, requiring a third order polynomial fit. The resulting calibration was used to resample the sensor data array to produce an idealized output array. Figures 3a and 3b show, respectively, the extracted reflectance curves before and after the wavelength calibration was applied. Sample spectra from the left side, the middle, and the right side of the swath are plotted.

3.3 Hyperion spectral measurements

As a pushbroom image spectrometer, Hyperion is also expected to exhibit spectral smile. Hyperion consists of two spectrographs, one covering the visible-near infrared (VNIR) wavelength range 357 nm to 1055 nm, the other, the short wave infrared (SWIR) 851 nm to 2576 nm. It outputs 220 spectral bands with an average 10 nm sampling interval and 10 nm nominal bandwidth. Measurements performed on all three data sets are shown in Figures 4a, 4b, 5a, and 5b.

Figure 4a displays the results for the oxygen feature at 761 nm and Figure 4b for the water vapour feature at 823 nm, both observed by the VNIR portion of the instrument. In Figure 4a, both the measurements and the corresponding second-order polynomial curve fits are displayed, while in Figure 4b, only the fitted curves are shown. Also plotted in Figures 4a and 4b respectively, are the laboratory calibration curves for the '763.14 nm' and '824.16 nm' Hyperion bands. Note that this designation is that used for the Coleambally data set and corresponds to the band-centre wavelength for the middle pixel. This designation has, for later data sets, been changed to a mean wavelength value for the band. For consistency, the former 'middle pixel' designation has been used here for all data sets.

The measurement results for the water vapour feature at 1136 nm are plotted in Figure 5a, overlaid by the corresponding second order polynomial curve fits. The second order polynomial fits for the carbon dioxide features at 1575-1607 nm are displayed in Figure 5b. Included in these figures are the laboratory calibrations for the '1134.45 nm' and '1578.37 nm' bands of the SWIR portion of Hyperion.
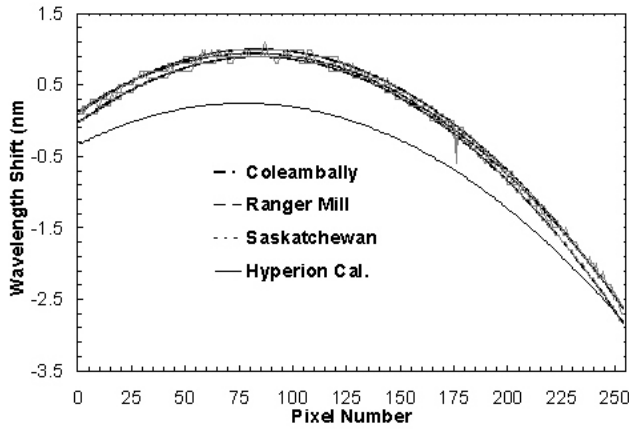
Figure 4a. Spectral smile measurements at the 761 nm oxygen absorption band, with their second order polynomial fits, for three Hyperion data sets. The laboratory calibration curve for the '763.14 nm' band is included for comparison.
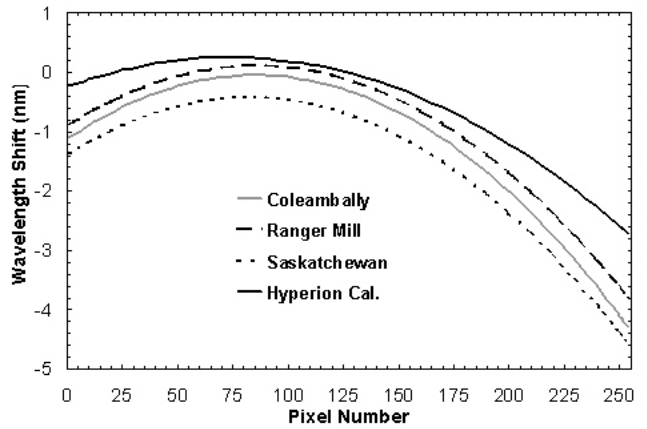
Figure 4b. Polynomial fits to the 823 nm water vapour absorption band for three Hyperion data sets. The laboratory calibration for the '824.16 nm' Hyperion band is included.
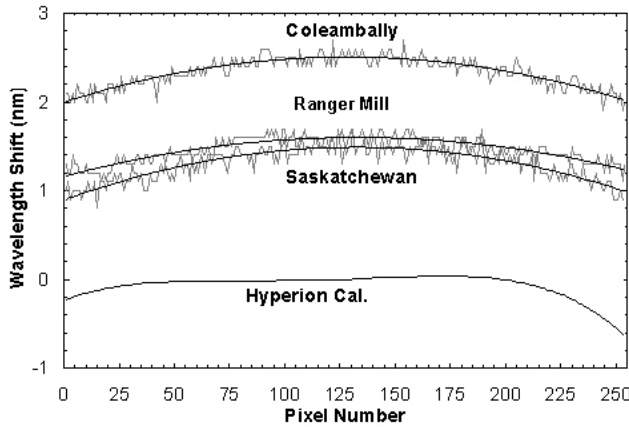
Figure 5a. Spectral smile measurements at the 1136 nm water vapour band, with their polynomial fits, for three Hyperion data sets. The laboratory calibration for the Hyperion '1134.45 nm' band is included.
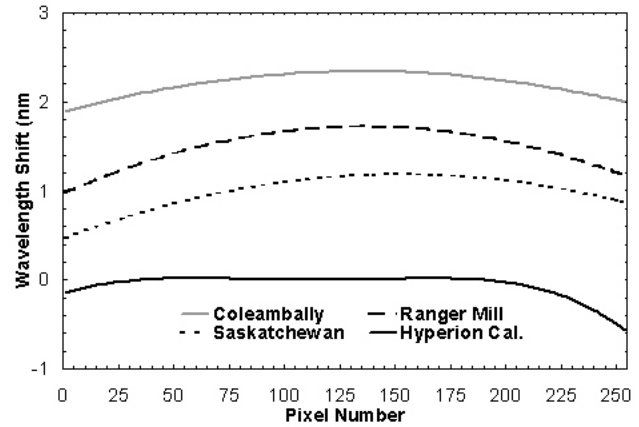
Figure 5b. Polynomial fits to the measured wavelength shift values at the carbon dioxide bands at 1575-1607 nm. The laboratory calibration curve for the '1578.37 nm' band is included for comparison.

In total, 10 features were used to establish a new wavelength calibration grid for both halves of the instrument. In Figure 6a, the reflectance spectra for pixels 3, 130, and 253, calculated using the laboratory band-centre values, are plotted. Displayed in Figure 6b are reflectance spectra for the same pixels, calculated using the measured values.

The mean shift values for each of the four absorption features, and for each of the three data sets were found by calculating the means-over-pixels of the differences between the curve fits to the measured values and the laboratory calibration values. These are listed in Table 3 along with the spectral smile amplitudes, both as specified by the laboratory calibrations and as measured. The differences in the smile amplitudes are also calculated, as are the standard deviations and the standard deviations of the mean fit.
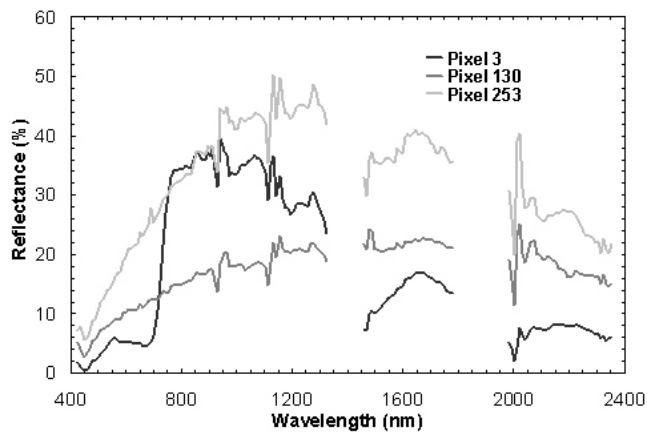
Figure 6a. Reflectance spectra calculated using the laboratory calibration values for the Hyperion band-centre wavelengths. Spectra from the Coleambally site represent both vegetation and soil.
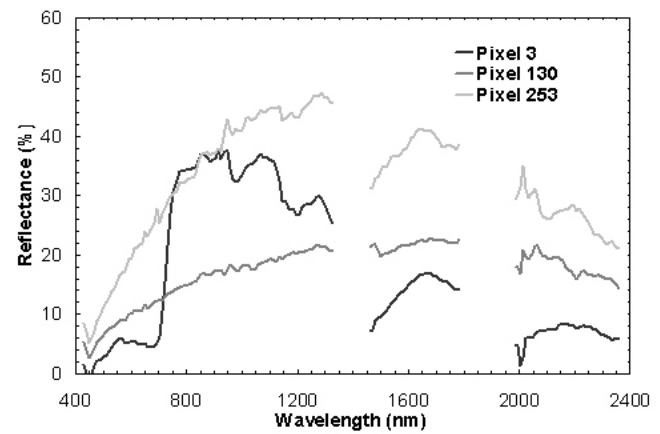
Figure 6b. Reflectance spectra from the same pixels calculated using the measured band-centre and bandwidth values for Hyperion. No smoothing has been done.

Scene Location and Date	Coleambally Jan 2002				Ranger Mill Mar 2002				Saskatchewan May 2002			
Absorption Feature & Wavelength (nm)	O_2 761	H_2O 823	H_2O 1136	CO_2 1575	O_2 761	H_2O 823	H_2O 1136	CO_2 1575	O_2 761	H_2O 823	H_2O 1136	CO_2 1575
Standard Deviation (nm) (Measurements vs Fit)	0.0352	0.0838	0.0726	0.2470	0.0464	0.0755	0.0695	0.2696	0.0521	0.1468	0.0908	0.2778
Standard Deviation of the Mean Fit (nm)	0.0022	0.0053	0.0046	0.0155	0.0029	0.0047	0.0044	0.0169	0.0033	0.0092	0.0057	0.0174
Mean Shift Measured – Lab (nm)	0.4807	-0.6109	2.4085	2.2571	0.6110	-0.3696	1.5322	1.5532	0.5669	-0.9676	1.3743	1.0492
Smile Amplitude as Measured (nm)	3.7237	4.2476	0.4998	0.4451	3.6350	3.9121	0.4396	0.7283	3.5778	4.1611	0.5874	0.7106
Smile Amplitude as per Lab Calibration (nm)	3.0600	2.9600	0.6800	0.5900	3.0600	2.9600	0.6800	0.5900	3.0600	2.9600	0.6800	0.5900
Smile Difference Measured – Lab (nm)	0.6637	1.2876	-0.1802	-0.1449	0.5750	0.9521	-0.2404	0.1383	0.5178	1.2011	-0.0926	0.1206

Table 3. Statistics for the spectral smile measure-ents made on the Hyperion data, for three data sets: Coleambally (Jan 2002), Ranger Mill (Mar 2002), and Saskatchewan (May 2002), each for four absorption features: oxygen (761 nm), water vapour (823 nm), water vapour (1136 nm), and carbon dioxide (1575-1607 nm). The listed shifts are obtained by calculating the means over the across-track pixels. The smile amplitudes are the ranges of the fitted polynomial curves.

4. DISCUSSION

4.1 Comparison of methods

The method most similar to that described here is the method used by Gao et al.[3] . The primary difference is the comparison metric used: Gao et al. uses the standard deviation between measured and modelled radiance spectra; our method uses the Pearson correlation coefficient. It is suggested that the amplitude invariance of the correlation coefficient offers an advantage.

Gao et al. do not describe how the underlying scene spectra are obtained, nor do they indicate whether any other preconditioning of the data has been performed to eliminate any impact of the scene reflectance on the measurement results. Nevertheless, the wavelength measurement results they have obtained for both AVIRIS and Hyperion data sets are comparable to the results obtained in the current work, and the pixel-to-pixel random variations are less in the Gao et al. results. More discussion of the source of these 'random' variations follows in section 4.3.

Another method employing modelled radiance spectra of atmospheric absorption lines is described by Barry et al.[2]. Their technique uses a cubic-spline curve fit to the measured radiance spectra followed by a determination of the wavelengths of the feature minima. They have estimated that the spline fit introduces errors of approximately 1 nm; our own investigations lead us to concur with this conclusion. As it is the conviction of the authors of the current work, as well as that of others, for example Gao et al., that the band-centre wavelength accuracies must be accurate to better than a fraction of a nanometre, it is clear that the method proposed by Barry et al. will not suffice.

4.2 AVIRIS test results

The AVIRIS data set was processed as a test of the procedure, with the expectation that the AVIRIS sensor, being a 'whiskbroom' instrument, would exhibit no spectral smile. While the measurements plotted in Figure 1a indicate pixel-to-pixel variations up to ±0.1 nm ($\sigma = 0.05$ nm), the second-order polynomial fit result indicates a maximum smile of only 0.018 nm. Results obtained by Gao et al. for AVIRIS for the same site, but for a different year (1995), are consistent with those obtained here, although their method does not involve the polynomial fit across pixels and so the results cannot be compared directly. The wavelength shift values found for the three water vapour bands all are within 0.5 nm of the nominal specified AVIRIS band wavelengths.

More importantly, as a test of the technique described here, the results obtained for AVIRIS indicate that the procedure is capable of making single pixel measurements down to ±0.05 nm with standard errors (standard deviation of the mean) in the AVIRIS case down to ±0.002 nm. It must be stated that these accuracies can be expected only for high signal-to-noise data in which across-track uniformity is not an issue. This point is discussed further in the next section. It is reiterated here that in these and following discussions of accuracies, it is assumed that the atmospheric absorption wavelengths contained in the atmospheric correction software are themselves accurate.

The technique described here is also capable of determining the bandwidths of the sensor, provided appropriate band response profile information is known *a priori*; in the present case a Gaussian response profile is assumed for AVIRIS. The bandwidth measurements in Figure 1b are plotted as a percent change relative to the specified bandwidth. A 2.06% ± 0.05% increase in bandwidth is indicated for the AVIRIS bands in the neighbourhood of the 942 nm water vapour absorption feature.

4.3 SFSI results

The SFSI results (Figure 2, Table 2) demonstrate the operation of the technique on data sets exhibiting large amplitude spectral line curvatures. The range and step size of the spectrum shifts used in constructing the convolved LUTs have been adjusted appropriately. The smile amplitudes in this case approach and exceed 18 nm; nevertheless, the technique provides band-centre wavelength accuracies which range from 0.03 nm down to 0.008 nm. It is noted that the smile curves are asymmetric; this indicates that the detector array is either not centred on the optic axis of the spectrograph, is rotated about the optic axis relative to the entrance slit, or both.

It is observed that the random pixel-to-pixel fluctuations vary from one spectral feature to another and from one part of the swath to another. While a portion of this variance may be attributed to sensor noise, in spite of attempts to minimise this source by averaging over a large number of frames (image lines) along-track, it cannot all be explained in this way; the signal-to-noise ratio for the data in the 1470 nm region is not as high as it is in the 2007 nm region, and yet, for pixels numbered higher than 300, the peak-to-peak variations are greater for the 2007 nm bands. It is hypothesized that one of the major sources of these fluctuations is the inadequacy of the spatial uniformity, and more specifically, the variation of this non-uniformity from spectral band to spectral band. The effects of random, temporal sensor noise can be reduced by averaging over more image frames along-track. The effects of non-uniformity can be reduced only by improving the uniformity coefficients. Contrast the results obtained for AVIRIS which has no spatial uniformity issues, since every measurement, for a given spectral band, is made with the same detector. Although there is no overlap of the AVIRIS and SFSI features reported here, and so an accurate comparison is not possible, it is noted that the lowest accuracy AVIRIS result is three times better than the highest accuracy SFSI result.

The impact of the application of the new band-centre and bandwidth calibration on the spectral reflectances displayed in Figures 3a and 3b is most significant. The improvements are apparent in the neighbourhoods of the 1268 nm oxygen band, the 1470 nm water vapour band, the 1575-1607 nm and 2005-2057 nm carbon dioxide bands, and water vapour bands at 2200 nm and 2300-2400 nm. Of these the 2005 nm and 2057 nm carbon dioxide features show the most spectacular improvements. It is noted that no smoothing has been done on these spectra.

4.4 Hyperion wavelength measurements

Since Hyperion is a pushbroom instrument, as is SFSI, one expects to observe spectral line curvature in these results. This is borne out by Figures 5 and 6 and Table 3; while the maximum measured smile amplitude for the Hyperion data sets is 4.25 nm, the shapes are similar to some of the SFSI smiles. Indeed the similarity extends to the asymmetry of the spectral curves, indicative of some type of opto-mechanical misalignment. The results contained in Figures 5 and 6 and Table 3 show significant differences between the measured and laboratory calibrated values, both in the overall shifts and in the smile amplitudes; in addition, for the SWIR features, the laboratory derived smile curves exhibit shapes that are at variance with the measured shapes. In all but the 823 nm feature, the measured shifts relative to the laboratory values are positive, i.e. the measured wavelength for a specific sensor band has shifted toward longer wavelengths.

One observes also that, except for the 761 nm oxygen feature, there are significant shifts amongst the measured values, and even for the 761 nm feature, the shift differences exceed the standard deviation of the mean fit (standard error), and hence cannot be attributed to random measurement error. It is noted that Gao et al.[3], also using a data set acquired over Colleambally, but on an earlier date, show smile curves for the 761 nm feature which are very similar to the results depicted in Figure 4a, including the negative spike at pixel 176. They indicate, for the earlier date, a peak shift of approximately 1 nm whereas we find a maximum shift of 0.66 nm. For the SWIR wavelengths, the shifts appear to correlate with data acquisition date, with the shift, relative to the laboratory calibration, decreasing in time. For the VNIR wavelengths, there is no correlation with date for the three data sets analysed in this work. Attempts to correlate the shifts with scene content have also been unsuccessful. Indeed, had such been the case, this dependance would have manifested itself in the Coleambally data, as this site consists of a mix of vegetated fields and freshly tilled fields. Neither is there any apparent correlation with latitude.

In comparing the calculated standard errors obtained for Hyperion to those for AVIRIS, it is noted that the Hyperion errors exceed the AVIRIS errors by factors of two and three for the 823 nm and 1136 nm bands respectively. As for the SFSI results discussed in Section 4.3, it is suspected that a primary source of the pixel-to-pixel fluctuations, apparent in the plots in Figures 4a and 5a, is the band-to-band mismatch of the spatial uniformity coefficients. In comparison with the SFSI results, the calculated error bars are general smaller, although there are no listed spectral features in common to permit a direct comparison.

The magnitudes of the shifts and the variations amongst data sets are significant, both in that they far exceed the error limits that can be explained by random measurement errors (the standard deviation of the mean fit) by factors exceeding 100, and also in that failure to incorporate these shifts into the data processing will lead to serious errors in the calculated reflectances.

The latter can be seen in Figure 6a where reflectance spectra from the Coleambally data set exhibit 'spikes' in the neighbourhoods of the water vapour features at 942 nm, 1136 nm, 1470 nm, and 2300-2350 nm, the oxygen feature at 1268 nm and the carbon dioxide features at 1575-1607 nm , 2007 nm and 2057 nm. These are most pronounced for the 942 nm, 1136 nm, 2005 nm and 2057 nm features. Most of these spikes are absent or significantly reduced in the reflectance spectra displayed in Figure 6b for which the measured band-centre values were used.

Only the 2005-2057 nm region retains spikes and these appear to be the result of the mis-compensation of the carbon dioxide absorption rather than a result of band-centre wavelength error. The 2057 nm feature is properly corrected for the lower reflectance spectrum, but moderately over-compensated for the higher reflectance cases; the 2005 nm feature ranges from seriously under-compensated for the lowest reflectance spectrum to over-compensated for the higher reflectance cases. These symptoms can be explained in part by an incorrect signal offset. The major improvements in the reflectance spectra constitute the ultimate confirmation of the validity of the new wavelength measurements.

5. SUMMARY

A technique has been described and demonstrated which permits the band-centre wavelengths and bandwidths to be measured using only the scene image data. At the heart of the method is the matching of measured spectral radiances with those derived using radiative transfer software, in this case MODTRAN 4.2. The method is capable of achieving accuracies of 0.002 nm. AVIRIS data has been used to test the method and to establish the accuracy limits. Data sets acquired by the SFSI airborne imaging spectrometer and the Hyperion satellite-borne instrument have been analysed using this method.

For Hyperion, three data sets acquired on three dates ranging from Jan 2002 to May 2002 have been processed and the results compared. The Hyperion results show band wavelength shifts, relative to the laboratory calibration values, which range from −1 nm to +0.6 nm for the VNIR instrument. For the SWIR instrument, shifts as high as 2.4 nm are measured. Comparison shows that the measured wavelength calibrations vary from data set to data set. The measured results vary up to 0.6 nm and 1.2 nm for the VNIR and SWIR instruments respectively.

Use of the measured band-centre and bandwidth calibrations in the atmospheric correction process to retrieve reflectance spectra from the SFSI and Hyperion radiance data is shown to give much improved results.

REFERENCES

1. D.J. Schroeder, *Astronomical Optics*, 14.1, Academic Press, San Diego, 2000.

2. P.S. Barry, J. Shepanski, and C. Segal, "Hyperion On-Orbit Validation of Spectral Calibration using Atmospheric Lines and On-board System", *Imaging Spectrometry VII*, M.R. Descour, S.S. Shen, editors, Vol. 4480, 231-235, SPIE, Bellingham, 2002.

3. B-C. Gao, M.J. Montes, and C.O. Davis, "A Curve-fitting Technique to Improve Wavelength Calibrations of Imaging Spectrometer Data", *Proceedings of the 11ʰ JPL Airborne Earth Science Workshop*, Robert O. Green, editor, JPL Publ. 03-4, 99-105, Jet Propulsion Laboratory, Pasadena, 2002.

4. A. Berk, L.S. Berstein, G.P. Anderson, P.K. Acharya, D.C. Robertson, J.H. Chetwynd, and S.M. Adler-Golden, "MODTRAN Cloud and Multiple Scattering Upgrades with Applications to AVIRIS", *Remote Sens. Environ.*, **65**, 367-375, 1998.

5. K. Staenz, and D.J. Williams, "Retrieval of Surface Reflectance from Hyperspectral Data Using a Look-Up Table Approach", *Canadian Journal of Remote Sensing*, **23**, 354-368, 1997.

6. R.O. Green, M.L. Eastwood, C.M. Sarture, T.G. Chrien, M. Aronsson, B.J. Chippendale, J.A. Faust, B.E. Pavri, C.J. Chovit, M. Solis, M.R. Olah, and O. Williams, "Imaging Spectrometry and the Airborne Visible/Infrared Imaging Spectrometer (AVIRIS)", *Remote Sensing of Environment*, **65**, 227-248, 1998.

7. R.A. Neville, N. Rowlands, R. Marois, and I. Powell, "SFSI: Canada's First Airborne SWIR Imaging Spectrometer", *Canadian Journal of Remote Sensing*, **21**, 328-336, 1995.

8. J. Pearlman, C. Segal, L.B. Liao, S. Carman, M. Folkman, W. Browne, L. Ong, and S.G. Ungar, "Development and Operations of the EO-1 Hyperion Imaging Spectrometer", *Earth Observing Systems V*, W.L. Barnes, editor, Vol. 4135, SPIE, Bellingham, 2000.